Cancer evolution in a changing microenvironment

Xiaowei Jiang* and Ian P.M. Tomlinson*

Cancer Genetics and Evolution Laboratory, Institute of Cancer and Genomic Sciences, College of Medical and Dental Sciences, Vincent Drive, University of Birmingham, Edgbaston, Birmingham B15 2TT, United Kingdom

*Corresponding authors: Xiaowei Jiang (x.jiang.4@bham.ac.uk), Ian P.M. Tomlinson (i.tomlinson@bham.ac.uk)

Abstract

Cancer development can be viewed as an evolutionary and ecological process, in which the tumour microenvironment (TME) is likely to play a critical role. Unfortunately, the TME is largely ignored or considered static in most cancer evolution models, and different cancers are often studied in isolation. A general theory of adaptive cancer evolution is lacking. Here we establish a phenotypic and genetic model of cancer evolution in three-dimensional (3D) space with a changing TME. With individual-based simulations, we show how cancer cells adapt to diverse changing TME conditions and fitness landscapes. Compared with static TMEs, changing TMEs can generate complex 3D dynamics of spatio-temporal heterogeneity involving variable subclonal fitness and mixing, driver mutations with different fitness effects and phylogenetic patterns. Our 3D simulations with changing TMEs capture some of the key morphological characteristics of cancer, including spatio-temporal ball-like and irregular clonal/subclonal population structures. A cycling TME, in particular, is capable of generating more driver mutations and promoting cancer adaptation. We predict that the TME is a major limiting factor of adaptive cancer evolution. Finally, our model can be used to simulate anti-cancer treatment strategies and show how they can be subverted by different resistance mechanisms. Our study provides an evolutionary and ecological framework for understanding cancer development and treatment, and provides novel insights into the processes of adaptive cancer evolution and precision cancer medicine.

Introduction

Understanding the mechanisms facilitating ecological adaptation is a fundamental question in evolutionary biology, including cancer development[1]. In 1976, Nowell outlined carcinogenesis as an evolutionary process using an illustrated phylogenetic model in which clonal and stepwise accumulation of advantageous mutations under selection from the tumour microenvironment (TME) was envisaged[2]. Our understanding of cancer development as an evolutionary process has increased greatly in the last decade due to advances in next generation sequencing and related analytical methods[3]. Many ideas and concepts originating in evolutionary biology and molecular evolution have become widespread in cancer research including gradual evolution with stepwise accumulation of driver mutations[4], punctuated evolution with "catastrophic" genomic changes[5] and neutral cancer evolution[6]. In some cases, anti-cancer treatment has been developed based on evolutionary principles[7]. Many interesting patterns have been observed based on single time point data from cancers at their time of surgical resection, such as spatial and temporal heterogeneity of subclonal mutations, subclonal mixing[8,9], and ball- and non-ball-like clonal and/or subclonal structures[10,11].

If the environment plays an important role in determining which somatic mutations drive tumour evolution under selection, the cancer cell and its TME should jointly determine the tumour evolutionary trajectory. Whilst the cancer cell may determine its own microenvironment to some extent, the source of selection extends to include many non-neoplastic cells, including various stromal components such as fibroblasts, immune cells, the extracellular matrix (ECM) and the pre-metastatic niche[12]. The TME is thought to be a dynamic regulator of tumour progression and metastasis[11,13-17]. Finally, the origin of cancer cells has been extended to both stem cells and non-stem cells[18,19].

Although the seminal ideas proposed by Nowell and others – that tumorigenesis proceeds by accumulating stepwise advantageous mutations under selection – have guided cancer research for decades, there is a lack of a general theory of adaptive cancer evolution. Some fundamental questions remain unanswered, including the role of the (changing) TME in determining the fitness effect of mutations and the evolutionary

trajectories of cancers in three-dimensional (3D) space. Does cancer evolution proceed by mutations with small fitness effects, large effects or a combination of both? How and why does the fitness effect of mutations differ across cancer types? Finally, what spatio-temporal patterns of cancer development can be observed under different tempos and modes of adaptive cancer evolution?

In previous cancer evolutionary modelling, in most cases the TME has been neglected and the fitness effect of mutations must therefore be pre-specified[6,10]. When the TME has specifically been considered as a source of selection, the underlying genetic basis [20-22], such as the variable fitness effects of adaptive mutations, have not been explicitly considered. Moreover, the important question of how cancer cells adapt in a changing TME has not generally been considered. To address these issues, we have analysed carcinogenesis as an adaptive evolutionary process, in which the cancer cell and its changing TME jointly determine the cancer evolutionary trajectory in 3D space, with the aim of providing a general theory of adaptive cancer evolution (see Methods for details). By simulating cancer growth in the 3D space of a changing TME in different fitness landscapes at single cell and population level, we identify various evolutionary patterns of 3D adaptive cancer evolution under diverse genetic, phenotypic, population genetic and changing TME conditions. We show that far more complex evolutionary patterns can emerge compared with models that assume a static TME. Important differences include the spatio-temporal heterogeneity in clonal/subclonal fitness, population mixing and structures, and the combination of driver mutations with various selective advantages[23].

Results

Description of the model

Our model uses formal adaptation theory and simple 3D growth dynamics, based on R.A. Fisher's geometric framework. This was originally described as the phenotypic geometric model in his seminal 1930 work "The genetical theory of natural selection", which provided much of our understanding of the nature of adaptation inherent in Darwin's theory of evolution by natural selection. The adaptive process Fisher described is analogous to adjusting the knobs of a microscope and each trait contributes to fitness

independently (universal pleiotropy)[24]. We assume that a changing TME in 3D leads to continual selection acting on the proliferation potential (the fitness effect) of mutations that influence the phenotypic traits of cancer cells. This is modelled by cancer fitness landscapes, with a single changing phenotypic optimum (v_1) determined by the TME (see Methods and Supplementary Figure S1).

In our model, each cancer cell is, for simplicity, diploid. We consider *n* traits and L loci. The number of traits is related to the notional phenotypic complexity of the cancer cell. It also determines the dimensionality of the fitness landscape, with a higher number of traits indicating a more "complex" cancer cell (for example, including more of the hallmarks of cancer[14], with traits such as aerobic glycolysis and immune evasion). In a very simple situation, the fitness of a cancer cell with two adaptive traits can be described by the fitness function in a three-dimensional Cartesian co-ordinate system, where the height along the fitness surface corresponds to fitness and the other two co-ordinates (Supplementary Figure S2) correspond to phenotypic values of each trait. The initial optimum phenotypic value defining the maximum fitness (the "peak" of the fitness landscape, see Supplementary Figure S2) is at the origin of the Cartesian coordinate system, and the optimum can move, directionally or otherwise (e.g., randomly or cyclically, see Methods), as the TME changes.

For a cancer cell, a phenotype, $\mathbf{z}$, of n traits is defined by a column vector, $\mathbf{z} = \left(z_1, ..., z_n\right)^T$ (equation (1)). We assume that the optimum, $\mathbf{z}^{opt} = \left(z_1^{opt}, ..., z_n^{opt}\right)^T$ (equation (2)) moves away from the origin following different dynamics (see Methods). So for a particular point representing a cancer cell's phenotype and fitness in the fitness landscape the Euclidean distance d between phenotype $\mathbf{z}$ and its optimum $\mathbf{z}^{opt}$ (equation (3)) and the fitness function $w(d)$ (equation (4)) determines the cancer cell's fitness (if epistasis is not considered). We assume each mutation affects all n traits according to the assumption in Fisher's geometric model. Each trait can then be changed with a certain probability by a random mutation, defined by a column vector, $\mathbf{r} = \left(r_1, ..., r_n\right)^T$ (equation (5)) that represents the phenotypic effect of the mutation at any of the 2L loci (see

Methods for details). The mutations in each generation additively determine the new n-dimensional phenotype $\mathbf{z}'$, which can then be changed again by further random mutations.

Both the moving phenotypic optimum of the TME and random mutations can change a cancer cell's fitness. For example, by equation (4), when the optimum moves away, the relative distance, d, will increase to d', which leads to a smaller fitness value $w(d')$. Similarly, a random mutation can also decrease or increase the phenotypic Euclidean distance to d' and lead to a new fitness $w(d')$, which may be higher or lower depending on the phenotypic effect of the random mutation. The phenotypic effect (size) of a mutation is sampled from a multivariate normal distribution (equation 11). A mutation with large fitness effect can move the cancer cell a long phenotypic distance relative to its phenotypic optimum in the fitness landscape. All these changes in fitness due to either mutational or TME effects naturally lead to different levels of selection and adaptation.

At each generation, a cancer cell is selected according to its fitness value and dies with probability $1-w(\mathbf{z},t)$, which depends on the phenotypic effects of the mutations in that cell and position of the TME optimum at time t. The surviving cancer cells reproduce asexually. New daughter cells randomly occupy available space in 3D according to pre-specified limits on tumour size. The tumour may go extinct, persist for a long time with varying size, or grow continuously until it reaches its maximum allowed space or size, after which it continues to be under viability selection without expanding. A cancer cell acquires higher fitness when mutation(s) move its phenotype to be closer to the optimum (defined by selection coefficient $s = w(\mathbf{r})/w(\mathbf{z}) > 0$). During the process, there are L allele trees used to keep track of alleles generated at each locus. If an allele becomes fixed in the population, we say this is an adaptive or positively selected mutation, even if subsequent TME changes render that mutation disadvantageous. This does not exclude the possibility that mutations may be "selected" due to linkage, including variants with negative fitness coupled to a mutation with a stronger positive effect. Competition between tumour sub-clones/cells may also occur naturally,

especially if there is a high mutation rate, such that cancer cells with different fitness carrying different beneficial mutations compete against each other for fixation (clonal interference).

We use computer simulations based on the above principles to assess cancer growth in 3D and look for patterns of adaptive cancer evolution. The initial fitness ($w_0 = w(\mathbf{z}_0)$) of the cancer cell is conferred by a starting phenotype, $\mathbf{z}_0$, which is pre-specified and could be determined by a new driver mutation or conceivably by phenotypic plasticity, which may, for example, arise from disturbances such as inflammation [13]. Mutation rates and the number of loci are also determined before each simulation: the mutation rate could, for example, be increased owing to mutations in key pathways maintaining DNA replication fidelity, or extrinsic mutagens; and the number of loci could also be increased or decreased, for example owing to changes in somatic copy number variation.

In the following sections, we first show how cancers adapt under the classic model of tumorigenesis, where the tumour is initiated from a single stem cell with high fitness, and we identify the general patterns of 3D spatio-temporal and adaptive cancer evolution in a dynamic TME with different rates of change. We then simulate cancer evolution following more general assumptions of tumour cell origin, such as different initial population sizes, phenotypes, fitness, and shapes of the fitness landscapes and other dynamics of TME change. Finally we show that our model can be used to demonstrate the effects of anti-cancer treatment strategies, such as radiotherapy, chemotherapy and immunotherapy, where the treatments can cause sudden or gradual changes in the TME optimum, thus changing the selection dynamics; we also show how different resistance mechanisms can subvert an apparently effective treatment.

Comparing adaptive cancer evolution in three dimensions under various changing and static TMEs

For simplicity we first assess the classic model of tumorigenesis in a *directionally* changing TME. A single cell with two traits ($n = 2$) starts asexual reproduction from the centre of the 3D tumour space with a phenotype at the origin with initial fitness $w_0 = 1$,

which could represent a stem cell with high fitness conferred by a driver mutation that starts to form a tumour in its local TME. The cancer starts to grow with cell birth probability, $w(\mathbf{z},t)$, and death probability, $1-w(\mathbf{z},t)$. The cancer may go extinct if it has low average fitness, while higher average fitness can keep the cancer persistent for long time.

In a static TME ($v_1 = 0$, the optimum does not move), the cancer can persist as long as an individual's natural life and it shows the classical constant stabilising selection, where the purifying selection is at play to remove individual cancer cells with deleterious mutations. Moreover, the mean cancer fitness remains high and does not fluctuate in 3D (Supplementary Movie S1). When the TME is changing initially our simulations show several interesting patterns of cancer clonal and/or subclonal growth, where the changing TMEs can generate complex spatio-temporal heterogeneity of cancer evolution.

First, we find that the fitness of cancer cells fluctuates through time and space showing complex 3D patterns (Supplementary Movies S2-S6). As in the model description this is due to mutation and a gradually changing TME that moves away the optimum of the fitness landscape – for example, resulting from a progressive chronic inflammation or simply from aging [13,25] – the fitness of each cancer cell changes accordingly (equation (9)). After viability selection, the surviving cells proliferate in 3D, leading to complex spatio-temporal patterns of cell birth and death, where different 3D morphologies of clonal or subclonal population structures emerge (see examples in Figures 1-2).

Second, we find that the speed of TME change plays a critical role in cancer progression and adaptation. Particularly, if the TME optimum moves too fast and the cancer cells do not acquire enough beneficial mutations to increase fitness, the population goes extinct (Supplementary Movies S2-S4). However, if the optimum moves at a moderate speed the cancer population may acquire enough beneficial mutations to "catch up" with the TME optimum (Supplementary Movies S5-S6). If the optimum moves slowly, the tumour can grow almost exponentially to the maximum space and/or population size allowed ($N = 10^7$), typically forming a ball (Supplementary Movies S5-S6), and then continue to evolve with a few adaptive mutations.

Third, we find two general clonal or sub-clonal growth patterns in 3D: (i) one or more balls of cells (Figure 1a-i); or (ii) irregular morphology (Figure 1j-l). Intriguingly, these patterns generally resemble those observed clinically [10,11]. It is more likely that ball-like clones or sub-clones are found in a fast-changing TME ($v_1 = 0.05$ and $v_1 = 5\times10^{-3}$, Figure 1a-f, Supplementary Movies S3 and S4) than a slow-changing TME ($v_1 = 5\times10^{-4}$ and $v_1 = 5\times10^{-5}$, Figure 1g-l, Supplementary Movies S5 and S6). Moreover, the fast-changing TMEs also lead to many smaller sub-clones, which turn over fast, with fluctuating numbers, spatial proximity and fitness (Figure 1a-c, Supplementary Movies S3). We also find that both spatio-temporal heterogeneity of sub-clones of different finesses, and sub-clonal mixing are frequently observed during cancer evolution (Figure 2a-l, Supplementary Movies S2-S6). In a relatively static or an extremely slow-changing TME the spatio-temporal clonal or sub-clonal turnover is slow and show irregular morphology more frequently (e.g., see Figure 1g-l, Supplementary Movies S6).

We then sought to understand the fitness effects of mutations fixed during cancer development under a changing TME. First, in a static TME, although the cancer can persist for an individual's natural life, we find that there is no fixation of any new driver mutations (Supplementary Figure S3 and Movies S1). Interestingly, this is a more general finding that might apply to the "Big Bang" model of colorectal tumor growth, which is characterised by a lack of selective sweeps and high intratumoural heterogeneity[6]. In a changing TME the mean population fitness and adaptive mutations are determined by the speed of TME change (Figure 3). As expected, the mean population fitness decreases faster in a fast-changing TME, whereas a slow-changing/static TME leads to slower fitness decay and thus longer survival time of the tumour (Figure 3a). Lower selection intensities (a "flatter" fitness landscape; Supplementary Figure S2) can mitigate against this problem, significantly extending the cancer's survival time to a period nominally as long as an individual's natural life (Supplementary Figures S4 and S5).

Second, in a fast-changing TME, the driver mutations that spread to fixation must have in general larger fitness effects (large selection coefficients, Figure 3b). This can be

explained from equations (12) and (13), as for an individual cancer cell, a faster changing optimum will produce relatively longer distances from its location to the optimum in the fitness landscape, thus reducing fitness and meaning that the cell is less likely to pass viability selection. In order to avoid extinction, cancer cells must continuously acquire mutations with larger fitness effects to catch up with the fast moving optimum, which becomes impossible when the TME changes too fast. These cancers can only survive for relatively short periods of time and harbour a few large adaptive mutations (Figure 3b-c, $v_1 = 0.5$, Supplementary Movie S2, $v_1 = 0.05$, mean selection coefficient: $s = 22\%$, Supplementary Movie S3, $v_1 = 5\times10^{-3}$, $s = 9\%$). Intriguingly, a moderately changing TME promotes cancer evolution with the highest number of adaptive mutations and relatively long survival time (Supplementary Movie S4 and $v_1 = 5\times10^{-4}$, mean selection coefficient: $s = 7\%$, Supplementary Movie S5).

Third, in a slowly changing TME, the mean selection coefficients of adaptive mutations are quite small (Figure 3b-c, $v_1 = 5\times10^{-5}$, mean selection coefficient: $s = 1\%$, Supplementary Movie S6). Interestingly, when the selection intensity decreases (increased width of the fitness landscape, see Supplementary Figure S2), the selection coefficients of fixed mutations become even smaller (e.g., with $\sigma^2 = 100$ and $v_1 = 5\times10^{-5}$, mean selection coefficient: $s = 0.3\%$, Supplementary Figure S4). This type of evolution by advantageous "nearly neutral" mutations with small fitness effect, as Tomoko Ohta pointed out, could be interpreted as adaptive evolution in a changing environment[26].

Finally, when the number of traits of cancer cells under selection increases from 1 to 8 (increase of cancer cell phenotypic complexity, n, see Methods), we find that there is a cost of complexity associated with cancer adaptive evolution. In particular, the mean fitness of the population decreases and the mean selection coefficient increases during adaptation when the cancer cell has an increased number of traits and changing TME (Figure 3d-e). This observation could be understood in terms of the hallmark traits of cancer cells[14]. Suppose that a tumour cell population "devotes" all its genetic variation to the adaptation of one or two key traits instead of eight traits, adaptation may become more efficient because there is no requirement for larger driver mutations. As a result

the cancer with lower phenotypic complexity may persist for longer period of time and it is more likely to establish a clinically significant cancer.

3D adaptive cancer evolution under diverse cancer initiation conditions and a changing TME

As stated above, a single cell with initial high fitness ($w_0 = 1$) due to driver mutations is almost guaranteed to initiate cancer growth under a directionally moving TME optimum. However, a cancer cell with lower fitness ($w_0 < 1$) may also initiate tumour growth under different TME changing directions and rates. To gain further insights, we now assume more general assumptions for cancer initiation and TME changing dynamics, such that the neoplastic growth is initiated by somatic cells with different initial phenotype/fitness and population sizes[19]. This can also serve as a model of metastasis in that migrating cells with different phenotypes and fitness must adapt at a distant site with a novel TME. In this general model, 3D cancer growth can in principle be initiated from any number of cells with any fitness in a TME that can take different types of changing dynamics.

We consider that the population starts from a phenotype away from the optimum, and thus has low initial fitness (equation (9), $w_0 < 1$). In order to avoid extinction (Supplementary Movie S7), a cancer must be initiated with a large population size when its initial fitness is very small (e.g., $w_0 = 0.1$) and initial driver mutations must occur with relatively large fitness effect (Figure 4a-d, Supplementary Movies S8-S11), which is true for both static and changing TMEs. In a static TME ($v_1 = 0$) when the initial cancer cell is away from the optimum (e.g., $w_0 = 0.6$) our simulation shows that only two driver mutations are recorded in subsequent adaptation (data not shown, similar to Figure 4e). This type of mutation should be considered to be classical drivers. This means that low fitness cells (a long phenotypic distance from the optimum) with a large initial population size have a higher chance of generating appropriate driver mutations to survive initial strong selection due to either sudden or rapid TME change. Higher fitness cells require few cells to initiate the neoplastic growth, which may be conferred by

either phenotypic plasticity or classical driver mutations already present in the initial transformed cells (movies not shown for $w_0 = 0.9$ as they evolve similarly to $w_0 = 1$, see Supplementary Movies S2-S6).

When the population survives its initial selection with driver mutations, its evolutionary trajectory still depends on the rate of TME change (Figure 4, Supplementary Movies S8-S15). Again our simulations show two similar patterns as above. First, a moderately changing TME promotes cancer adaptation by fixing more driver mutations (Figure 4b, f and j, Supplementary Movies S9, S13). Second, if the population evolves under a slowly changing TME, we recover subsequent driver mutations that have small fitness effects (Figure 4a, e and i, Supplementary Movies S7, S15). These mutations could be termed "mini-drivers", as we proposed previously[23]. Interestingly, this phenomenon resembles the pattern of Fisher's micromutationism, in which adaptation proceeds initially by mutations of larger fitness effect and subsequently smaller fitness effect mutations[27] predominate when the phenotype approaches the optimum (assuming that the TME optimum moves quite slowly, Figure 4).

In cancer evolution, most driver mutations have pleiotropic effects, affecting multiple pathways and several cancer traits. Although we assumed that each mutation affects all traits (universal pleiotropy), its fitness effect on each trait may be different. In other words, the driver mutations may have different fitness effects on different traits and the selection is therefore correlated (equation (9)), which can be illustrated by the shapes of the fitness landscapes with different levels of correlation (see Supplementary Figure S2). Similarly, a mutation (genotype) may have different phenotypic effects on each trait. So the mutational effects on traits can be independent or correlated (see mutational distribution, equation (11)). Indeed, we find that when the TME changes slowly, the fitness effects of driver mutations along traits indeed correlate (Supplementary Figure S6). Moreover, we find that when the TME changes fast the phenotypic effects of driver mutations along traits have similar levels of correlation as correlations of mutational effects (data not shown). Although in clinical settings the effects of selectional and mutational correlations on cancer progression are unclear, an example may be multiple

mutations in Wnt signalling pathway genes (APC, TCF7L2, SOX9) in colorectal cancer, or multiple mutations in Pi3K genes (e.g. KRAS and PIK3CA) in several cancers.

Finally, to understand how other TME changing dynamics may affect cancer adaptation we analysed another three types of changing TME. First, when the TME changes randomly, the resulting increase in the TME variance at different time points always acts against cancer adaptation (equations (14)-(16)), leading to reduced mean population fitness and a requirement for adaptive mutations with higher mean fitness effect (Supplementary Figure S7). Second, when we add a random component into a directionally changing TME (equations (17)-(19)), the increased variance caused by the random component also acts against cancer adaptation, producing similar results to a purely randomly changing TME (Supplementary Figure S8). Third, when the TME changes cyclically (equations (20)-(22)), with increased amplitude, the cycling TME optimum also acts against cancer adaptation (Supplementary Figure S9). However, interestingly, although the mean population fitness decreases and mean selection coefficient of adaptive mutations increase when the amplitude increases, there are more adaptive mutations recorded than under any other TME changing dynamics (full data not shown, amplitude $A = 4$, see Supplementary Figure S9 and Supplementary Movies S16-S17). Moreover, there are also more complex spatio-temporal patterns of sub-clonal fitness and mixing, in which birth and death of large and small sub-clones with diverse fitness values occur frequently through time and space (Supplementary Movies S16-S17). This indicates that a cycling TME at intermediate level may be particularly capable of promoting cancer adaptation by periodically fixing more adaptive mutations than TMEs that change directionally and/or randomly.

We then reconstructed cancer phylogenies in the three types of simulations. Intriguingly, we found that in all cases the shape and the temporal signals in the phylogenies (e.g., the branch length and overall shape) were characteristic of its particular TME changing dynamics, such as static, directional, random and cyclic TMEs with different optimum changing speed (illustrated and explained in Supplementary Figure S10). These patterns from cancer phylogenies could be particularly useful in inferring the underlying TME selection dynamics and cancer evolutionary history.

Cancer adaptation owing to anti-cancer therapies

Anti-cancer therapies of all sorts, but principally those that are non-surgical, introduce an artificial TME that can radically change the tumour's selective landscape, at least transiently and possibly permanently. In the case of targeted therapies, for example, cells with a beneficial mutation can rapidly become at a selective disadvantage. As a proof of concept, we find that our model can be used to understand anti-cancer therapies that use different dosing strategies, by assuming that these modify the TME selective optimum and/or the shape of the fitness landscape (see equations (25)-(28), Supplementary Figure S2). Initially, we have examined treatments that cause a sudden change in the TME optimum, such as genotoxic therapies (radiotherapy or chemotherapy)[28] and immunotherapy[29] (e.g. immune checkpoint inhibitors), which should put strong selective pressure on all cancer cells.

For simplicity, we assume that the therapy causes the TME optimum to move suddenly along the axis of a single trait. We first assume that the cancer has evolved to a constant TME optimum $z_0^{opt} = 0$ and allow it 100 generations to accumulate genetic variation and reach maximum tumour size ($N = 1 \times 10^7$). We then assess four different TME optima to represent different treatment strategies ($z_1^{opt} = 5,6,7,8$, see equations (25)-(28), Supplementary Movies S18-S21) that treat the cancer for about 33 months or more (e.g., 1000 generations), reducing mean population fitness below $w = 0.1$. We illustrate how the optimum of the fitness landscape changes from z_0^{opt} to z_1^{opt} under each treatment (Supplementary Figure S11).

As shown in Figure 5, all treatments reduce the fitness of all cancers below $w = 0.1$ (Figure 5a-o) and at $z_1^{opt} = 8$ the cancer is successfully cured (the population is extinct, Figure 5p), but due to mutation and smaller TME change (e.g., because of smaller dose or effectiveness of the delivery) the cancers survive at $z_1^{opt} = 5,6,7$ and quickly relapse in less than two months (Figure 5p). In general, when the dose is not sufficient for maximum killing, smaller effective doses lead to selection for mutations with smaller

fitness effects, while higher doses lead to the opposite. Phylogenetic trees show that treatment selection often leads to expansion of sub-clones and extinction of the majority of the tumour mass (Figure 5e, j and o). Weak treatment $z_1^{opt} = 5$ leads to a large number of initial sub-clones with resistant beneficial mutations, but eventually the tumour mass comes to be dominated by a single sub-clone (Figure 5e) carrying the mutation with the largest fitness effect ($s = 5.19$). Stronger, but non-lethal, treatment ($z_1^{opt} = 7$) leads to an early sub-clonal expansion carrying the mutation with a very large selection coefficient ($s = 26.563$, Figure 5o).

In terms of sub-clonal diversity, we first observe a reduction soon after treatment and then an increase of diversity, but after the sub-clonal fitness recovers to the same/similar levels as pre-treatment or with minor loss, the diversity reduces again until the end of the treatment (data not shown). These behaviours are consistent with a mean fitness decrease due to the treatment and selection for resistant sub-clones (Figure 5p). Interestingly, our simulations show that both pre-existing and *de novo* resistant mutations can be observed. Moreover, when the treatments lead to higher selection intensity (a "narrower" fitness peak, see Supplementary Figure S2), all treatments lead to immediate cure (population extinction).

To understand potential therapeutic resistance, we examined three mechanisms that cancers could use to avoid population extinction (Supplementary Movies S22-S24, Supplementary Figure S12). First, we assume a polygenic model of resistance, which has quantitative traits. Increasing the number of loci contributing to resistance can avoid extinction with one positively selected mutation (e.g., $L = 50$, Supplementary Figure S12a). Second, with an elevated mutation rate – perhaps caused by the therapy itself – the population fitness can quickly rebound and avoid extinction, which leads to two positively selected mutations (Supplementary Figure S12b). Interestingly, all three fixed mutations have a *de novo* origin after treatment initiation because all other mutations in sub-clones may have been removed by therapeutic selection or fail to hitchhike within the dominant sub-clone. Third, if the selection intensity decreases, for example therapy intensity reduces owing to toxicity, the cancer population can also avoid extinction ($\sigma^2 = 40$, Supplementary Figure S12c, the fitness landscape shape change is illustrated in

Supplementary Figure S11). Nevertheless, due to weaker selection, no positively selected mutations are detected. The resistant sub-clones generally arise early after treatment and the complex growth patterns of the 3D resistant sub-clones are striking, including mixing and fast turnover (Supplementary Figure S12d, Supplementary Movies S22-S24).

We now combine our findings from our general model of cancer evolution with those of the evolutionary responses to anti-cancer therapy. Treatment strategies that lead to a moving TME optimum (in any direction) may be effective and help to reduce toxicity by using of a lower dose, as there is no requirement of initial maximum dosing to induce a high sudden optimum change for maximum killing (Figure 5, Supplementary Figure S13). The strategy is theoretically as effective as the classical maximum dosing in reducing mean cancer cell fitness (similar to Supplementary Movies S2-S4, Supplementary Figure S13), although it takes longer time. Fast-moving TME optima cause eventual extinction and thus successful treatment, although other changing TME dynamics (equations (14)-(22)) can also reduce cancer fitness and cause cancer extinction (Supplementary Figure S7-S9, Supplementary Movies S16-S17). Moreover, dosing strategies should, in principle, be optimized individually depending on the maximum allowed dose tolerance and the type of cancer (see Supplementary Figure S7-S9, Supplementary Movies S1-S3). So a trade off may be required between the theoretical dose for maximum killing and the actual patient drug tolerance. For instance, in directional dosing the treatment must be stopped when the allowed dose is reached or continue if the tolerance is increased. Since moving TME-based anti-cancer strategies are highly desirable, designing clinically effective dosing and delivery strategies is important, although currently challenging.

Discussion

In this study, we provide an evolutionary and ecological framework for understanding cancer development and anti-cancer treatment strategies. This framework captures the complex 3D spatio-temporal dynamics of intra-tumour heterogeneity in sub-clonal fitness and structure, and the tempo and mode of adaptive cancer evolution in a changing TME. Cancer evolution appears to be far more complex in a changing TME (e.g.,

Supplementary Movies S1-S6, S16-S17), particularly as regards the early stages, including rapid sub-clonal shifts and "spontaneous" regression or tumour death, which suggests there are many unobservable failed evolutionary trajectories of cancer progression in human patients unless caught prior to extinction[17]. Our model is thus biologically interpretable and intuitive, as parameters of birth, death and selection are naturally incorporated into the properties of the TME and the underlying phenotypic effect of mutations.

Currently the actual fitness effects of most mutations in cancer genomes are unknown, although estimates suggest that selection is often weak, even for major driver mutations[30]. Our model predicts that there are many mutations with small fitness effects due to weak selection caused by a slowly or moderately changing TME. These mutations may be pervasive in current cancer genomic data but are difficult to identify due to their small effects. Our study gives a theoretical basis to the observed weak selection, and may help to explain why cancers are rarer than would be predicted given the number of cells in the body and the potential role of the TME in restraining cancer progression[17]. Many cancer driver mutations might be classified as "nearly neutral"[31] as described by Tomoko Ohta[26]. However, as Tomoko Ohta pointed out, due to a changing environment, it is appropriate to classify fixed advantageous mutations as positively selected, even when their fitness effect is quite small. So it is appropriate to term these mutations as "mini drivers"[23].

Adaptive cancer evolution in individuals may have several evolutionary tempos and modes mixed across cancer types in humans, which can be explained by the heterogeneity of the TME and its varying optimum. On one hand, cancer cells may frequently go to extinction due to strong stabilizing selection from the normal TME. On the other hand, an extremely slow-changing or constant TME may lead, in effect, to limited cancer cell evolution in which neutral/nearly neutral mutations accumulate, as might be the case for cancers that apparently carry no or few classical driver mutations. Of course, the TME may determine the phenotypic effect of a mutation as well as determine the selective landscape, so a changing TME might alter both a phenotype and its selective advantage. Furthermore, cancer growth and progression (e.g. acquisition of new mutations) will also affect the TME; and the cancer itself may create or modify a

TME optimum leading to non-cell-autonomous cancer evolution. Therefore, quantitative understanding of these basic components and TME changing dynamics in individual patients is crucial for developing future cancer medicine. For instance, we show that a cycling TME may be particularly capable of promoting cancer adaptation (see Supplementary Movies S16-S17 for its unusual long-term sub-clonal dynamics and a large number of recorded adaptive steps), while stochasticity and fast changes in the TME may act against cancer adaptation. TME dynamics need to be considered alongside other factors in studies that aim to provide a complete picture of the underlying cancer evolutionary dynamics.

In this study we show that in a moderately/slowly changing/static TME, lifetime seeding is possible to distant sites (e.g., see Figure 3a and 3b, $v_1 = 5\times10^{-4}$ and $v_1 = 5\times10^{-5}$), but successful colonization at distant metastatic sites is stochastic and uncertain, because it depends on the initial phenotype and population size of the circulating cancer cells and their interactions with the distant metastatic TMEs (or pre-metastatic niches) assuming that metastatic potential depends on the long survival of the primary cancer due to a slowly changing TME (Figure 4). Phenotypic plasticity may play a role in initial adaptation, which confers higher fitness of initial cells with a small migrating population (Figure 4i-l). This is consistent with the hypothesis that the pre-metastatic niche may bring the phenotype of the migrating cancer cells closer to the optimum of a potential metastatic TME for higher fitness[12,15,32]. There is empirical evidence that cancer cells migrate in small numbers. Metastasis does not necessarily require that circulating cancer cells have major driver mutations to initiate cancer adaptation[33] as shown in Figure 4i. Although in a static TME our observation does support the main characteristics of the "Big Bang" model, we show that the main evolutionary force at play in this situation is likely to be weak purifying selection[34]. Our simulations may also capture some of the unobservable aspects of cancer development, which may happen before the "Big Bang".

Current cancer data are mostly derived from relatively late stages of cancer development, where the cancer has accumulated large heterogeneity under weak dynamic selection possibly due to a changing TME. Although the initial classic driver

mutations with large fitness effect can be easily detected using next generation sequencing, the fitness effect of such mutations under a changing TME remains unclear in clinical settings, which leads to scenarios where no obvious drivers can be detected with current approach when the fitness effect of these driver mutations is small. This poses significant challenges for cancer treatment. Our results support the use of proposed therapeutic strategies that can target the TME, causing to change, and drive cancer cell populations to extinction[17,35]. Importantly, the TME dynamics required to kill cancer cells may be different for each individual patient, which will further require precise and individualised modelling of therapeutic dosage and delivery strategies. Although a similar approach, termed "adaptive therapy", has been proposed previously[36], where treatments have been adjusted by evolutionary principles and there is clear evidence of improved patient outcome by cyclic dosing [37], the true evolutionary dynamics of cancer progression and treatment can only be understood by combined measures of cancer genetic and phenotypic changes and the corresponding TME dynamics, as we demonstrate in this study.

In conclusion, our 3D model provides a natural evolutionary and ecological framework to understand adaptive cancer evolution. We show that the extension of Fisher's classical model using fitness landscapes with a changing TME is sufficient to produce many of the observed complex cancer evolutionary and 3D pathology patterns. In the future, *in vivo* and/or *in vitro* experiments, combined with such modelling approaches and fine-scale methods, such as single-cell sequencing and phylogenetics, could be used to elucidate cancer fitness landscapes with dynamic TMEs, further testing the (un)predictability of cancer evolution, with implications for cancer precision medicine[38].

Methods

Model

In evolution, organisms can evolve in a Darwinian or non-Darwinian way or a combination of both depending on how natural selection acts on the phenotypic traits and their plasticity[39]. The fitness advantage to organisms conferred by these traits due to environmental selection can lead to adaptation[40-42]. However, adaptation may not

simply be a consequence of natural selection, as the plasticity/robustness of the phenotypes and the underlying molecular underpinnings may be responsible[27,39,40,43-45]. For instance, a plausible path of adaption, which involves both plasticity and selection, starts with the initial plastic adaptation (initial fitness advantage) and subsequent stabilizing selection and/or positive selection due to environmental changes[15,39,46]. These evolutionary theories help to define a general mode of cancer initiation and subsequent adaptation. In this study, we follow Fisher's geometric framework[27,47-49]. To address the question of how cancer cell populations adapt to a changing environment, we extended the original Fisher geometric model into a general form incorporating a moving environmental optimum with different changing dynamics[31,49-51]. This framework has not previously been applied to study carcinogenesis as an adaptive evolution process in a changing tumour microenvironment.

In Fisher's geometric framework a cancer cell adapting in a tumour microenvironment can be viewed as a point in an n-dimensional Euclidean phenotype space with n quantitative phenotypic traits defined by a column vector $\mathbf{z}$

$$\mathbf{z} = \left(z_1, \ldots, z_n\right)^T . \quad (1)$$

The traits involved can be any, but could for convenience be those highlighted by Hanahan and Weinberg[14]: sustaining proliferative signaling, evading growth suppressors, resisting cell death, enabling replicative immortality, angiogenesis, activating invasion and metastasis, reprogramming of energy metabolism and evading immune destruction[14]. The number of traits or the dimension of the phenotypic vector, n, represents the "complexity" of a cancer cell. As we assume that the TME (the ecology) is the primary source of selection[17,51-56], there is a corresponding optimum phenotype $\mathbf{z}^{opt}$, which is defined by a column vector of n values

$$\mathbf{z}^{opt} = \left(z_1^{opt}, \ldots, z_n^{opt}\right)^T . \quad (2)$$

The Euclidean distance, d, is defined as

$$
\begin{aligned}
d &= \left\| \mathbf{z} - \mathbf{z}^{opt} \right\|, \\
&= \sqrt{\left(z_1 - z_1^{opt}\right)^2 + \left(z_2 - z_2^{opt}\right)^2 + \cdots + \left(z_n - z_n^{opt}\right)^2}, \quad (3) \\
&= \sqrt{\sum_{k=1}^{n} (z_k - z_k^{opt})^2}.
\end{aligned}
$$

The phenotypic fitness function for a cancer cell in a microenvironment is defined as[49]

$$
\begin{aligned}
w(d) &= \exp\left(-ad^2\right), \\
&= \exp\left(-a\left\| \mathbf{z} - \mathbf{z}^{opt} \right\|^2\right).
\end{aligned} \quad (4)
$$

Here a is the selection intensity for all traits ($a > 0$)[49]. Therefore, the fitness of an individual cancer cell depends on its phenotype's Euclidean distance to the optimum. Equation (4) suggests that the closer a cancer cell's phenotype is to the optimum, the fitter it becomes. The change of phenotypic traits of a cancer cell due to random mutations can be defined as an n-dimensional random number:

$$
\mathbf{r} = \left(r_1, \ldots, r_n\right)^T, \quad (5)
$$

the size of a mutation (the effect of a mutation on phenotypic traits) is therefore defined as

$$
\left\| \mathbf{r} \right\| = \sqrt{r_1^2 + r_2^2 + \cdots + r_n^2}, \qquad (6)
$$

so the combined phenotypic trait of a cancer cell $\mathbf{z}'$ with mutation $\mathbf{r}$, relative to its wild type $\mathbf{z}$ is defined as

$$\mathbf{z}' = \mathbf{z} + \mathbf{r}, \qquad (7)$$

the selection coefficient of a mutation that changes the fitness of the cancer cell is therefore defined as

$$s \equiv \frac{w(\mathbf{z}')}{w(\mathbf{z})} - 1 = \frac{w(\mathbf{z}+\mathbf{r})}{w(\mathbf{z})} - 1, \quad (8)$$

when $s > 0$ the mutation is beneficial, it moves the cancer cell closer to the optimum. When the cancer cell is at optimum we say it has its maximum fitness $w(\mathbf{z}) = 1$, whereas when the cancer cell moves away from the optimum its fitness decreases and it could reach its lowest fitness $w(\mathbf{z}) = 0$. Such mutations are deleterious and lead to negative selection coefficients with $s < 0$. When mutations do not change fitness, they are defined as neutral mutations with $s = 0$.

We can now define a general form of the fitness function from equation (4) as shown before[24,47,48,57].

$$w(\mathbf{z},t) = \exp\left[-\left(\mathbf{z} - \mathbf{z}^{opt}(t)\right)^T \mathbf{S}^{-1}\left(\mathbf{z} - \mathbf{z}^{opt}(t)\right)\right], \quad (9)$$

where $\mathbf{S}$ is a real $n \times n$ positive definite and symmetrical matrix, and T denotes transposition. The matrix $\mathbf{S}$ describes the shape of the fitness landscape, namely, the selection intensity. Matrix $\mathbf{S}^{-1}$ is the inverse of $\mathbf{S}$. As introduced above, the overlapping of pathways responsible for cancer cell traits indicates pleiotropic effect of mutations

contributing to cancer adaptive evolution[14]. If the selection intensity is the same along all n traits then we have an isotropic fitness landscape (universal pleiotropy). We set $\mathbf{S}=\sigma^2\mathbf{I}$ ($\sigma^2>0$, $\mathbf{I}$ is an identity matrix). Selection may also vary along different traits (selection is correlated), which means mutational effects contribute to fitness differently for different traits. If we set selection intensity to vary along n traits, then $\mathbf{S}$ has non-zero off-diagonal entries. We illustrate different shapes of the fitness landscape (independent and correlated selection, Supplementary Figure S2). We can use $\bar{\sigma}^2=\sqrt[n]{\det(\mathbf{S})}$ to measure the average width of the fitness landscape, where $\bar{\sigma}^2$ is defined as the geometric mean of the eigenvalues of $\mathbf{S}$. The selection coefficient of a mutation in equation (8) can now be defined as

$$s(\mathbf{z},\mathbf{z}',t)=\frac{w(\mathbf{z}',t)}{w(\mathbf{z},t)}-1. \qquad (10)$$

Distribution of mutation effect size

We assume the phenotypic effect of a mutation with size $\mathbf{r}$ follows a multivariate normal distribution with mean $\mathbf{0}$ and $n\times n$ variance-covariance matrix $\mathbf{M}$[48,58]:

$$P(\mathbf{r})=\frac{1}{\sqrt{(2\pi)^n\det(M)}}\exp\left(-\frac{1}{2}\mathbf{r}'\mathbf{M}^{-1}\mathbf{r}\right), \qquad (11)$$

as above $\mathbf{M}$ is also symmetrical and positive-definite. We have $\mathbf{M}=m^2\mathbf{I}$, where m^2 is the variance of mutational effects and $\mathbf{I}$ is an identity matrix. If mutational effects are correlated we have covariance of mutational effects as the off diagonal elements in $\mathbf{M}$.

The average variance of mutational effects, $\bar{m}^2$, is given by the geometric mean of the eigenvalues of $\mathbf{M}$. We have $\bar{m}^2 = \sqrt[n]{\det(\mathbf{M})}$.

Cancer adaptation in a changing microenvironment

In all, we consider six scenarios for the properties of the tumour microenvironment. Different initial population or individual cell properties (e.g., population size and fitness) during computer simulations are specified in the results section. We assume that the TME optimum of the first trait of the n traits changes[48,50].

1. Directionally changing optimum

We assume a directionally moving optimum with $\mathbf{v}t$

$$\mathbf{z}^{opt}(t) = \mathbf{v}t, \quad (12)$$

$$w(\mathbf{z},\mathbf{v},t) = \exp\left[-(\mathbf{z}-\mathbf{v}t)^T \mathbf{S}^{-1}(\mathbf{z}-\mathbf{v}t)\right], \qquad (13)$$

where the vector $\mathbf{v} = (v_1,\ldots,v_n)'$ is the TME change speed. The optimum $\mathbf{z}^{opt}(t)$ is time (generation) dependent and only the first trait optimum changes.

2. Randomly changing optimum

Here we assume the TME optimum of the first trait, z_1^{opt}, changes randomly at each generation, t, following a Normal distribution with mean 0 and standard deviation, δ

$$\mathbf{z}^{opt}(t) = (z_1^{opt},\ldots,z_n^{opt}), \quad (14)$$

$$z_1^{opt} \sim N(0,\delta^2), \qquad (15)$$

$$w(\mathbf{z},t) = \exp\left[-(\mathbf{z}-\mathbf{z}^{opt}(t))^T \mathbf{S}^{-1}(\mathbf{z}-\mathbf{z}^{opt}(t))\right]. \qquad (16)$$

3. Directionally changing optimum, with a random component

We assume a directionally moving optimum with $\mathbf{v}t$ (see equation (12)) and a random component $\mathbf{e}$

$$\mathbf{z}^{opt}(t) = \mathbf{v}t + \mathbf{e}, \qquad (17)$$

$$\varepsilon_1 \sim N\left(0,\delta^2\right), \quad (18)$$

$$w\left(\mathbf{z},\mathbf{v},\mathbf{e},t\right)=\exp\left[-\left(\mathbf{z}-\mathbf{z}^{opt}\left(t\right)\right)^T \mathbf{S}^{-1}\left(\mathbf{z}-\mathbf{z}^{opt}\left(t\right)\right)\right], \quad (19)$$

where $\mathbf{v}=\left(v_1,...,v_n\right)'$ is the vector of the TME change and it is time dependent. The random vector $\mathbf{e}=\left(\varepsilon_1,...,\varepsilon_n\right)'$ has ε_1 following a random normal distribution with mean 0 and standard deviation δ.

4. Cyclically changing optimum

In this scenario, we assume the TME optimum changes cyclically or periodically at each generation, t, following a general periodic function[50,58,59]

$$\mathbf{z}^{opt}\left(t\right)=\left(z_1^{opt}(t),...,z_n^{opt}(t)\right), \quad (20)$$

$$z_1^{opt}(t)=\frac{A}{2}\left[1+\sin\left(\frac{2\pi t}{P}-\frac{\pi}{2}\right)\right], \quad (21)$$

$$w\left(\mathbf{z},t\right)=\exp\left[-\left(\mathbf{z}-\mathbf{z}^{opt}\left(t\right)\right)^T \mathbf{S}^{-1}\left(\mathbf{z}-\mathbf{z}^{opt}\left(t\right)\right)\right], \quad (22)$$

where A is the amplitude of TME optimum oscillation and P is the period (the number of generations) of the TME cycle. The equation (21) allows the TME optimum to change periodically from 0 to A and then to 0 in P generations. In all simulations of this scenario P is fixed at 360 generations.

5. Stable (i.e. constant) optimum

We assume the microenvironment optimum is constant with $\mathbf{z}_0^{opt}$:

$$\mathbf{z}^{opt}\left(t\right)=\mathbf{z}_0^{opt}=\left(z_1,...,z_n\right), \quad (23)$$

$$w\left(\mathbf{z}\right)=\exp\left[-\left(\mathbf{z}-\mathbf{z}_0^{opt}\right)^T \mathbf{S}^{-1}\left(\mathbf{z}-\mathbf{z}_0^{opt}\right)\right]. \quad (24)$$

6. Sudden change in the optimum

We assume the TME optimum suddenly changes from $\mathbf{z}_0^{opt}$ to $\mathbf{z}_1^{opt}$:

$$\mathbf{z}^{opt}(t) = \mathbf{z}_0^{opt} = \left(z_0^{opt},...,0\right), \qquad (25)$$

$$\mathbf{z}^{opt}(t) = \mathbf{z}_1^{opt} = \left(z_1^{opt},...,0\right), \qquad (26)$$

$$w(\mathbf{z}) = \exp\left[-\left(\mathbf{z}-\mathbf{z}_0^{opt}\right)^T \mathbf{S}^{-1}\left(\mathbf{z}-\mathbf{z}_0^{opt}\right)\right], \qquad (27)$$

$$w(\mathbf{z}) = \exp\left[-\left(\mathbf{z}-\mathbf{z}_1^{opt}\right)^T \mathbf{S}^{-1}\left(\mathbf{z}-\mathbf{z}_1^{opt}\right)\right]. \qquad (28)$$

In this scenario, the cancer cells evolve under constant stabilizing selection in the TME with optimum $\mathbf{z}_0^{opt}$, and after a sudden change the cancer cells then evolve under another constant stabilizing selection with a new optimum $\mathbf{z}_1^{opt}$ (the optimum of the first trait changes from z_0^{opt} to z_1^{opt}).

Simulation of cancer evolution in the three-dimensional space

Our intention was to identify key cancer evolutionary patterns in 3D and investigate how these are influenced by model parameters, such as the number of phenotypic traits n (the complexity of cancer cells), changing microenvironment (properties of the TME), selection correlation, population size, mutation rate, initial phenotype/fitness of cancer cells (distance to optimum), initial population size and chromosome instability affect 3D cancer adaptation (tumorigenesis) in an ecological and evolutionary framework.

We simulate the cancer cell population in 3D space in one of the six environments described above (Supplementary Figure S1). The simulation is fully individual-based, following simple growth mechanics[10,60]. In brief, the offspring of newly divided cells stochastically look for available positions in a 3D lattice space. The population evolves in a discrete and non-overlapping manner. The empty 3D tumour space represents the tumour microenvironment that may change, following the dynamics described above, and the position in the 3D space does not affect the TME or selection.

Simulations are performed under particular TME change patterns due to either natural cause or anti-cancer therapies as described in equations (12)-(28). The number of traits is fixed in each simulation at $n=1$ to $n=8$. Here we assume cancer cells require at least

one adaptive trait for survival (e.g. anti-apoptotic or metabolism related traits) as also inspired by microbial adaptive evolution[61] and mammals with very low cancer incidencies[62,63]. The initial population has K neoplastic cells, and grows from the centre of the specified 3D coordinates in the 3D square lattice (it has 26-cell cubic neighbours, also called a 3D Moore neighbourhood) until it reaches the defined maximum population size or 3D tumour space. The initial K cells have an adjustable phenotype $\mathbf{z}_0$. This determines the initial fitness in the fitness landscape, which has the optimum at the origin and an adjustable shape defined by $\mathbf{S}$ in equation (9) (illustrated in Supplementary Figure S2). The initial phenotype can also be calculated by equation (9) when the predefined fitness value is known. For generality we consider that the adjustable phenotype of initial K cells is determined by either classical driver mutations or by phenotypic plasticity.

The cancer cells have c sets of chromosomes (ploidy) and reproduce asexually with chromosome instability (CIN) (Supplementary Figure S1). To model CIN for simplicity we define a rate, r_c, to vary the copy of paternal and maternal chromosome passed down to daughter cells. Each individual cancer cell is represented by L diploid loci (for computational efficiency without loss of generality $c=2$, $L=5$, unless stated otherwise) with additive effect on the n-dimensional phenotype $\mathbf{z}$.

A multifurcating tree tracks the genealogies of the alleles generated at these loci. When only one branch of an allele tree survives an adaptive step is recorded as per standard terminology[48]. The per locus mutation rate, $u=4\times10^{-5}$, is used for per genome replication [64]. Due to high mutation rate and large population size multiple mutations may be generated in each generation. So there is clonal interference in our simulations. For this reason we only use individual-based simulations in our study. Analytical results concerning equations (12)-(28) have previously been reported[48,49,56,65,66]. At each generation cancer cells are removed with probability $1-w(\mathbf{z})$ as viability selection. In each simulation the population genetics parameters are recorded and displayed in real-time on the computer screen including time in years with 24 hours doubling time (can be adjusted if required), adaptive steps, generation time and population size. The reason

to set the doubling time as 24 hours is to allow simulations of more generation time to gain more insights into the underlying evolutionary process (e.g., one day doubling time allows roughly 37000 generations for 100 years, however, 5 days doubling time only allows about 7400 generations). The summary statistics for population fitness and adaptive steps are sampled every 100 generations unless otherwise stated. The real-time spatial evolutionary process of the cancer development is visualized in 3D. Two-dimensional (2D) or 3D snapshots including fitness values of each cancer cell and movies are made directly from simulations. The phylogeny of the evolving cancer cells in each simulation can be reconstructed in real-time by removing dead cells. The related simulations in this study took over 60 computer core years (equivalent to one computer core runs non-stop for 60 years) to finish.

Author contributions

XJ and IPMT conceived the study. XJ developed the model and implemented the computational framework and performed the simulations. XJ and IPMT analysed the simulation results. XJ and IPMT wrote the manuscript.

Acknowledgements

XJ is supported by an ERC advanced grant (EVOCAN-340560) awarded to IPMT. We thank John Welch and Sebastian Matuszewski for discussion, and Sebastian Matuszewski and Andrea Sottoriva for providing their publication materials. We are grateful to Shazia Irshad and members of the Tomlinson laboratory for cancer biology discussions. We thank Robert Esnouf and Jonathan Diprose from Oxford Wellcome Trust Centre for Human Genetics Research Computing Core for computing assistance.

References

1 Merlo, L. M., Pepper, J. W., Reid, B. J. & Maley, C. C. Cancer as an evolutionary and ecological process. *Nat Rev Cancer* **6**, 924-935, doi:10.1038/nrc2013 (2006).

2 Nowell, P. C. The clonal evolution of tumor cell populations. *Science* **194**, 23-28 (1976).

3 Gerlinger, M. *et al.* Cancer: evolution within a lifetime. *Annu Rev Genet* **48**, 215-236, doi:10.1146/annurev-genet-120213-092314 (2014).

4 Vogelstein, B. & Kinzler, K. W. The multistep nature of cancer. *Trends Genet* **9**, 138-141 (1993).

5 Navin, N. *et al.* Tumour evolution inferred by single-cell sequencing. *Nature* **472**, 90-94, doi:10.1038/nature09807 (2011).

6 Sottoriva, A. *et al.* A Big Bang model of human colorectal tumor growth. *Nat Genet* **47**, 209-216, doi:10.1038/ng.3214 (2015).

7 Enriquez-Navas, P. M. *et al.* Exploiting evolutionary principles to prolong tumor control in preclinical models of breast cancer. *Sci Transl Med* **8**, 327ra324, doi:10.1126/scitranslmed.aad7842 (2016).

8 de Bruin, E. C. *et al.* Spatial and temporal diversity in genomic instability processes defines lung cancer evolution. *Science* **346**, 251-256, doi:10.1126/science.1253462 (2014).

9 McPherson, A. *et al.* Divergent modes of clonal spread and intraperitoneal mixing in high-grade serous ovarian cancer. *Nat Genet* **48**, 758-767, doi:10.1038/ng.3573 (2016).

10 Waclaw, B. *et al.* A spatial model predicts that dispersal and cell turnover limit intratumour heterogeneity. *Nature* **525**, 261-264, doi:10.1038/nature14971 (2015).

11 Lan, C. *et al.* Quantitative histology analysis of the ovarian tumour microenvironment. *Sci Rep* **5**, 16317, doi:10.1038/srep16317 (2015).

12 Liu, Y. & Cao, X. Characteristics and Significance of the Pre-metastatic Niche. *Cancer Cell* **30**, 668-681, doi:10.1016/j.ccell.2016.09.011 (2016).

13 Quail, D. F. & Joyce, J. A. Microenvironmental regulation of tumor progression and metastasis. *Nat Med* **19**, 1423-1437, doi:10.1038/nm.3394 (2013).

14 Hanahan, D. & Weinberg, R. A. Hallmarks of cancer: the next generation. *Cell* **144**, 646-674, doi:10.1016/j.cell.2011.02.013 (2011).

15 Zhang, L. *et al.* Microenvironment-induced PTEN loss by exosomal microRNA primes brain metastasis outgrowth. *Nature* **527**, 100-104, doi:10.1038/nature15376 (2015).

16 Hawkins, E. D. *et al.* T-cell acute leukaemia exhibits dynamic interactions with bone marrow microenvironments. *Nature* **538**, 518-522, doi:10.1038/nature19801 (2016).

17 Bissell, M. J. & Hines, W. C. Why don't we get more cancer? A proposed role of the microenvironment in restraining cancer progression. *Nat Med* **17**, 320-329, doi:10.1038/nm.2328 (2011).

18 Schwitalla, S. *et al.* Intestinal tumorigenesis initiated by dedifferentiation and acquisition of stem-cell-like properties. *Cell* **152**, 25-38, doi:10.1016/j.cell.2012.12.012 (2013).

19 Davis, H. *et al.* Aberrant epithelial GREM1 expression initiates colonic tumorigenesis from cells outside the stem cell niche. *Nat Med* **21**, 62-70, doi:10.1038/nm.3750 (2015).
20 Anderson, A. R., Weaver, A. M., Cummings, P. T. & Quaranta, V. Tumor morphology and phenotypic evolution driven by selective pressure from the microenvironment. *Cell* **127**, 905-915, doi:10.1016/j.cell.2006.09.042 (2006).
21 Gatenby, R. A. & Gillies, R. J. A microenvironmental model of carcinogenesis. *Nat Rev Cancer* **8**, 56-61, doi:10.1038/nrc2255 (2008).
22 Lloyd, M. C. *et al.* Darwinian Dynamics of Intratumoral Heterogeneity: Not Solely Random Mutations but Also Variable Environmental Selection Forces. *Cancer Res* **76**, 3136-3144, doi:10.1158/0008-5472.CAN-15-2962 (2016).
23 Castro-Giner, F., Ratcliffe, P. & Tomlinson, I. The mini-driver model of polygenic cancer evolution. *Nat Rev Cancer* **15**, 680-685, doi:10.1038/nrc3999 (2015).
24 Waxman, D. & Welch, J. J. Fisher's microscope and Haldane's ellipse. *Am Nat* **166**, 447-457, doi:10.1086/444404 (2005).
25 de Magalhaes, J. P. How ageing processes influence cancer. *Nat Rev Cancer* **13**, 357-365, doi:10.1038/nrc3497 (2013).
26 Ohta, T. The Nearly Neutral Theory of Molecular Evolution. *Annu Rev Ecol Syst* **23**, 263-286 (1992).
27 Orr, H. A. The genetic theory of adaptation: a brief history. *Nat Rev Genet* **6**, 119-127, doi:10.1038/nrg1523 (2005).
28 Barnett, G. C. *et al.* Normal tissue reactions to radiotherapy: towards tailoring treatment dose by genotype. *Nat Rev Cancer* **9**, 134-142, doi:10.1038/nrc2587 (2009).
29 Fridman, W. H., Zitvogel, L., Sautes-Fridman, C. & Kroemer, G. The immune contexture in cancer prognosis and treatment. *Nat Rev Clin Oncol*, doi:10.1038/nrclinonc.2017.101 (2017).
30 Vermeulen, L. *et al.* Defining stem cell dynamics in models of intestinal tumor initiation. *Science* **342**, 995-998, doi:10.1126/science.1243148 (2013).
31 Razeto-Barry, P., Diaz, J. & Vasquez, R. A. The nearly neutral and selection theories of molecular evolution under the fisher geometrical framework: substitution rate, population size, and complexity. *Genetics* **191**, 523-534, doi:10.1534/genetics.112.138628 (2012).
32 Patel, S. A. & Vanharanta, S. Epigenetic determinants of metastasis. *Mol Oncol*, doi:10.1016/j.molonc.2016.09.008 (2016).
33 Makohon-Moore, A. P. *et al.* Limited heterogeneity of known driver gene mutations among the metastases of individual patients with pancreatic cancer. *Nat Genet* **49**, 358-366, doi:10.1038/ng.3764 (2017).
34 Noorbakhsh, J. & Chuang, J. H. Uncertainties in tumor allele frequencies limit power to infer evolutionary pressures. *Nat Genet* **49**, 1288-1289, doi:10.1038/ng.3876 (2017).
35 Tauriello, D. V. F. & Batlle, E. Targeting the Microenvironment in Advanced Colorectal Cancer. *Trends in Cancer*, doi:10.1016/j.trecan.2016.08.001 (2016).
36 Gatenby, R. A., Silva, A. S., Gillies, R. J. & Frieden, B. R. Adaptive therapy. *Cancer Res* **69**, 4894-4903, doi:10.1158/0008-5472.CAN-08-3658 (2009).
37 Zhang, J., Cunningham, J. J., Brown, J. S. & Gatenby, R. A. Integrating evolutionary dynamics into treatment of metastatic castrate-resistant prostate cancer. *Nat Commun* **8**, 1816, doi:10.1038/s41467-017-01968-5 (2017).

38 Bank, C., Matuszewski, S., Hietpas, R. T. & Jensen, J. D. On the (un)predictability of a large intragenic fitness landscape. *Proc Natl Acad Sci U S A* **113**, 14085-14090, doi:10.1073/pnas.1612676113 (2016).
39 Hughes, A. L. Evolution of adaptive phenotypic traits without positive Darwinian selection. *Heredity* **108**, 347-353, doi:10.1038/hdy.2011.97 (2012).
40 Fisher, R. A. *The genetical theory of natural selection*. (The Clarendon press, 1930).
41 Wright, S. The roles of mutation, inbreeding, crossbreeding, and selection in evolution. *Proceedings of the Sixth International Congress of Genetics* **1**, 356-366 (1932).
42 Haldane, J. B. S. *The causes of evolution*. (Longmans, Green and co., 1932).
43 Waddington, C. H. Genetic Assimilation of an Acquired Character. *Evolution* **7**, 118 (1953).
44 Wagner, G. P., Booth, G. & Bagheri, H. C. A population genetic theory of canalization. *Evolution* **51**, 329-347, doi:Doi 10.2307/2411105 (1997).
45 Pigliucci, M., Murren, C. J. & Schlichting, C. D. Phenotypic plasticity and evolution by genetic assimilation. *J Exp Biol* **209**, 2362-2367, doi:10.1242/jeb.02070 (2006).
46 Ghalambor, C. K. *et al.* Non-adaptive plasticity potentiates rapid adaptive evolution of gene expression in nature. *Nature* **525**, 372-375, doi:10.1038/nature15256 (2015).
47 Martin, G. & Lenormand, T. A general multivariate extension of Fisher's geometrical model and the distribution of mutation fitness effects across species. *Evolution* **60**, 893-907 (2006).
48 Matuszewski, S., Hermisson, J. & Kopp, M. Fisher's geometric model with a moving optimum. *Evolution* **68**, 2571-2588, doi:10.1111/evo.12465 (2014).
49 Tenaillon, O. The Utility of Fisher's Geometric Model in Evolutionary Genetics. *Annu Rev Ecol Evol Syst* **45**, 179-201, doi:10.1146/annurev-ecolsys-120213-091846 (2014).
50 Fraisse, C., Gunnarsson, P. A., Roze, D., Bierne, N. & Welch, J. J. The genetics of speciation: Insights from Fisher's geometric model. *Evolution* **70**, 1450-1464, doi:10.1111/evo.12968 (2016).
51 Lourenco, J. M., Glemin, S. & Galtier, N. The rate of molecular adaptation in a changing environment. *Mol Biol Evol* **30**, 1292-1301, doi:10.1093/molbev/mst026 (2013).
52 Tomlinson, I. Mutations, evolutionary theory and cancer. *Trends Ecol Evol* **8**, 107-110, doi:10.1016/0169-5347(93)90062-T (1993).
53 Tomlinson, I. & Bodmer, W. Selection, the mutation rate and cancer: ensuring that the tail does not wag the dog. *Nat Med* **5**, 11-12, doi:10.1038/4687 (1999).
54 Junttila, M. R. & de Sauvage, F. J. Influence of tumour micro-environment heterogeneity on therapeutic response. *Nature* **501**, 346-354, doi:10.1038/nature12626 (2013).
55 Waxman, D. & Peck, J. R. Sex and adaptation in a changing environment. *Genetics* **153**, 1041-1053 (1999).
56 Kopp, M. & Hermisson, J. The genetic basis of phenotypic adaptation II: the distribution of adaptive substitutions in the moving optimum model. *Genetics* **183**, 1453-1476, doi:10.1534/genetics.109.106195 (2009).
57 Waxman, D. Fisher's geometrical model of evolutionary adaptation--beyond spherical geometry. *J Theor Biol* **241**, 887-895, doi:10.1016/j.jtbi.2006.01.024 (2006).

58 Zhang, X. S. Fisher's geometrical model of fitness landscape and variance in fitness within a changing environment. *Evolution* **66**, 2350-2368, doi:10.1111/j.1558-5646.2012.01610.x (2012).
59 Charlesworth, B. Directional selection and the evolution of sex and recombination. *Genet Res* **61**, 205-224 (1993).
60 Sottoriva, A., Spiteri, I., Shibata, D., Curtis, C. & Tavare, S. Single-molecule genomic data delineate patient-specific tumor profiles and cancer stem cell organization. *Cancer Res* **73**, 41-49, doi:10.1158/0008-5472.CAN-12-2273 (2013).
61 Elena, S. F., Cooper, V. S. & Lenski, R. E. Punctuated evolution caused by selection of rare beneficial mutations. *Science* **272**, 1802-1804 (1996).
62 Seluanov, A. *et al.* Hypersensitivity to contact inhibition provides a clue to cancer resistance of naked mole-rat. *Proc Natl Acad Sci U S A* **106**, 19352-19357, doi:10.1073/pnas.0905252106 (2009).
63 Sulak, M. *et al.* TP53 copy number expansion is associated with the evolution of increased body size and an enhanced DNA damage response in elephants. *Elife* **5**, doi:10.7554/eLife.11994 (2016).
64 Bozic, I. *et al.* Accumulation of driver and passenger mutations during tumor progression. *Proc Natl Acad Sci U S A* **107**, 18545-18550, doi:10.1073/pnas.1010978107 (2010).
65 Kopp, M. & Hermisson, J. The genetic basis of phenotypic adaptation I: fixation of beneficial mutations in the moving optimum model. *Genetics* **182**, 233-249, doi:10.1534/genetics.108.099820 (2009).
66 Martin, G. & Lenormand, T. The fitness effect of mutations across environments: Fisher's geometrical model with multiple optima. *Evolution* **69**, 1433-1447, doi:10.1111/evo.12671 (2015).

Figure Legends

Figure 1. 3D simulation snapshots of cancer adaptive evolution under various directionally changing TME optima.

Illustrative 3D snapshots of the evolving cancer cell population are taken sequentially, under different TME change rates (see Methods), v_1. **a-c**, $v_1 = 0.05$. **d-f**, $v_1 = 5\times10^{-3}$. **g-i**, $v_1 = 5\times10^{-4}$. **j-l**, $v_1 = 5\times10^{-5}$. Cancer cells are coloured according to their fitness (≥0.75, red, <0.75 green). Note that, because of immediate population extinction, data are not shown for simulations with TME change rate at $v_1 = 0.5$. The width of the fitness landscape (i.e. selection intensity) is set to $\sigma^2 = 10$ (equation (9) and Supplementary Figure S2).

Figure 2. 3D simulation snapshots of cancer evolution under various directionally changing TME optima with different fitness cut-off values to illustrate sub-clonal heterogeneity of fitness.

Illustrative 3D snapshots of the evolving cancer cell population are taken with different fitness cut-off values from Figure 1a, 1d, 1g and 1j. Cancer cells are coloured according to their fitness cut-off value, which results in two colours for the 3D snapshots: red (large than or equal to cut-off value indicating higher fitness) and green (small than cut-off value indicating lower fitness), respectively. The cut-off value for fitness is 0.75 for (**a, d**). The cut-0ff value for fitness is 0.9 for (**b, e**). The cut-off value for fitness is 0.99 for (**c, f**), (**g, j**), (**h, k**) and (**i, l**). Note that the lower fitness cancer cells are coloured in green with low colour opacity in **d**, **e**, **f**, **j**, **k** and **l**. The corresponding original figures are in **a**, **b**, **c**, **g**, **h**, and **i**, respectively.

Figure 3. Representative cancer evolution trajectories with different rates of directionally changing TME optima.

a, the mean population fitness of the evolving cancer cells is sampled at various TME change rates . The dashed line represents mean fitness 0.5. When mean population fitness reaches this value it is more likely to be extinct. The line represents a simple linear regression fit. **b**, the mean selection coefficients are sampled at various TME

change rates. The line represents a smooth curve. **c**, the mean selection coefficients are plotted against the TME change rates. **d**, the mean population fitness is plotted against the number of traits of cancer cells. **e**, the mean selection coefficients are plotted against the number of traits of cancer cells. The TME rates used are $v_1 = 0.5$, $v_1 = 0.05$, $v_1 = 5\times10^{-3}$, $v_1 = 5\times10^{-4}$ and $v_1 = 5\times10^{-5}$. Note that, because of immediate population extinction data are not shown for simulations with TME change rate at $v_1 = 0.5$. Error bars are the standard error of the mean (s.e.m.), and each point represents 100 independent simulations.

Figure 4. Cancer evolution under multiple different initial conditions.
Simulations are performed with different initial conditions regarding population size, fitness and TME change rates. Three conditions for initial population size are used, $N = 10$ (coloured blue), $N = 10^4$ (coloured red) and $N = 10^7$ (coloured green), respectively. Three conditions for initial fitness are also used, $w = 0.1$ (**a-d**), $w = 0.5$ (**e-h**) and $w = 0.9$ (**i-l**). Populations also evolve under four different TME change rates: $v_1 = 5\times10^{-5}$ (**a, e** and **i**), $v_1 = 5\times10^{-4}$ (**b**, **f** and **j**), $v_1 = 5\times10^{-3}$ (**c**, **g** and **k**) and $v_1 = 0.05$ (**d**, **h** and **l**), respectively. Error bars are s.e.m. and each point represents 100 independent simulations. Note that in **e-l** all color lines are present, but they are too close to each other to be seen clearly.

Figure 5. Cancer evolution under different anti-cancer treatment strategies.
Example 3D snapshots are taken sequentially after sudden change of the TME optimum due to treatments (**a-o**). Four different treatments maintaining four different levels of TME optimum are shown: $z_1^{opt} = 5$ (**a-e**), $z_1^{opt} = 6$ (**f-j**), $z_1^{opt} = 7$ (**k-o**) and $z_1^{opt} = 8$ (no 3D snapshots are taken due to immediate population extinction after treatment), respectively. For understanding clonality of cancer cells after treatments, **e**, **j** and **o** show the clonal expansion of cancer cells after treatments for $z_1^{opt} = 5$, $z_1^{opt} = 6$ and $z_1^{opt} = 7$, respectively. In order to track the precise fitness status of the population the sample is taken for every generation. The population fitness plotted against generation time is

summarized in **p** for each treatment, and the dashed line indicates when the treatment starts (after generation 100).

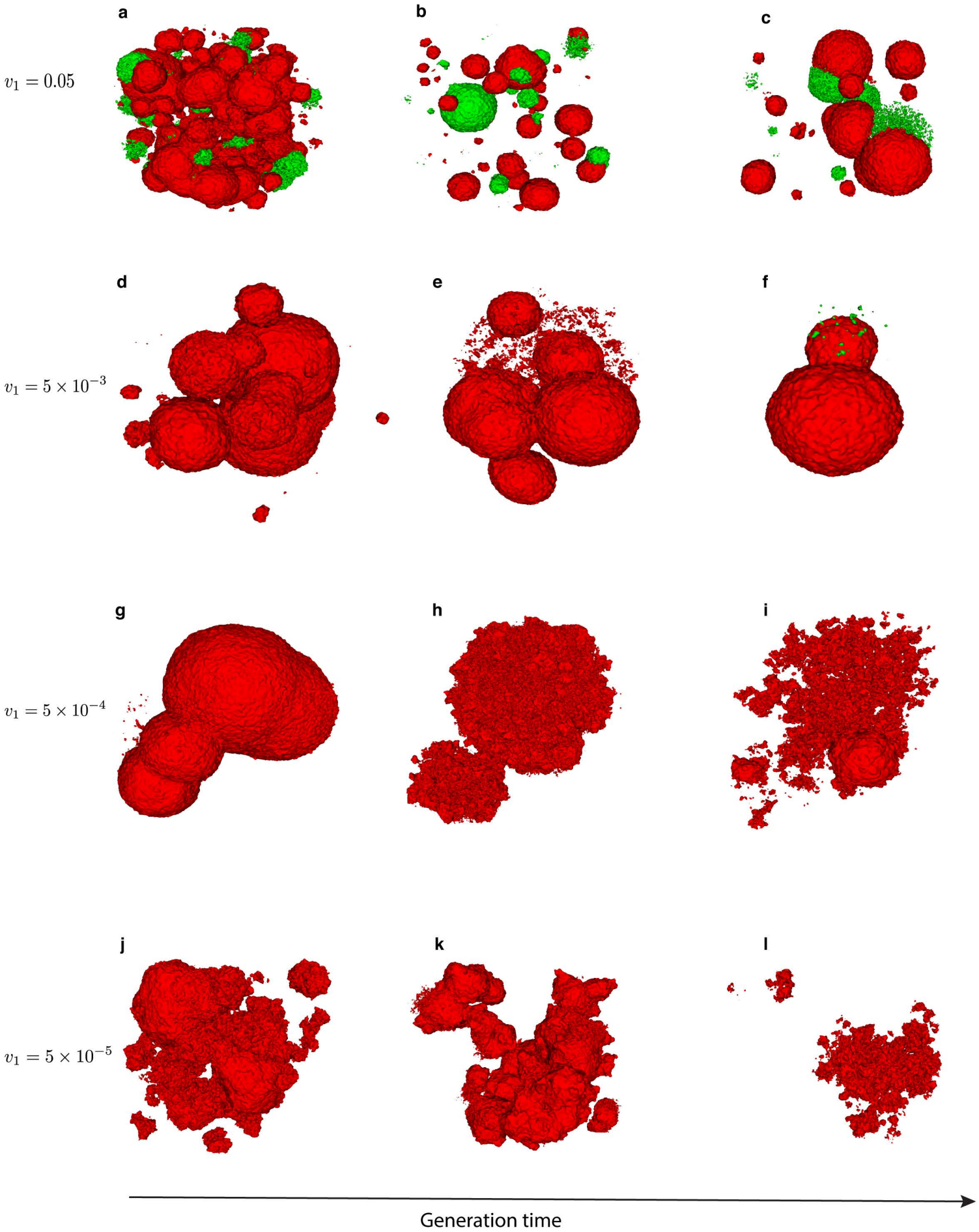
a
b
c
$v_1 = 0.05$
d
e
f
$v_1 = 5 \times 10^{-3}$
g
h
i
$v_1 = 5 \times 10^{-4}$
j
k
l
$v_1 = 5 \times 10^{-5}$
Generation time

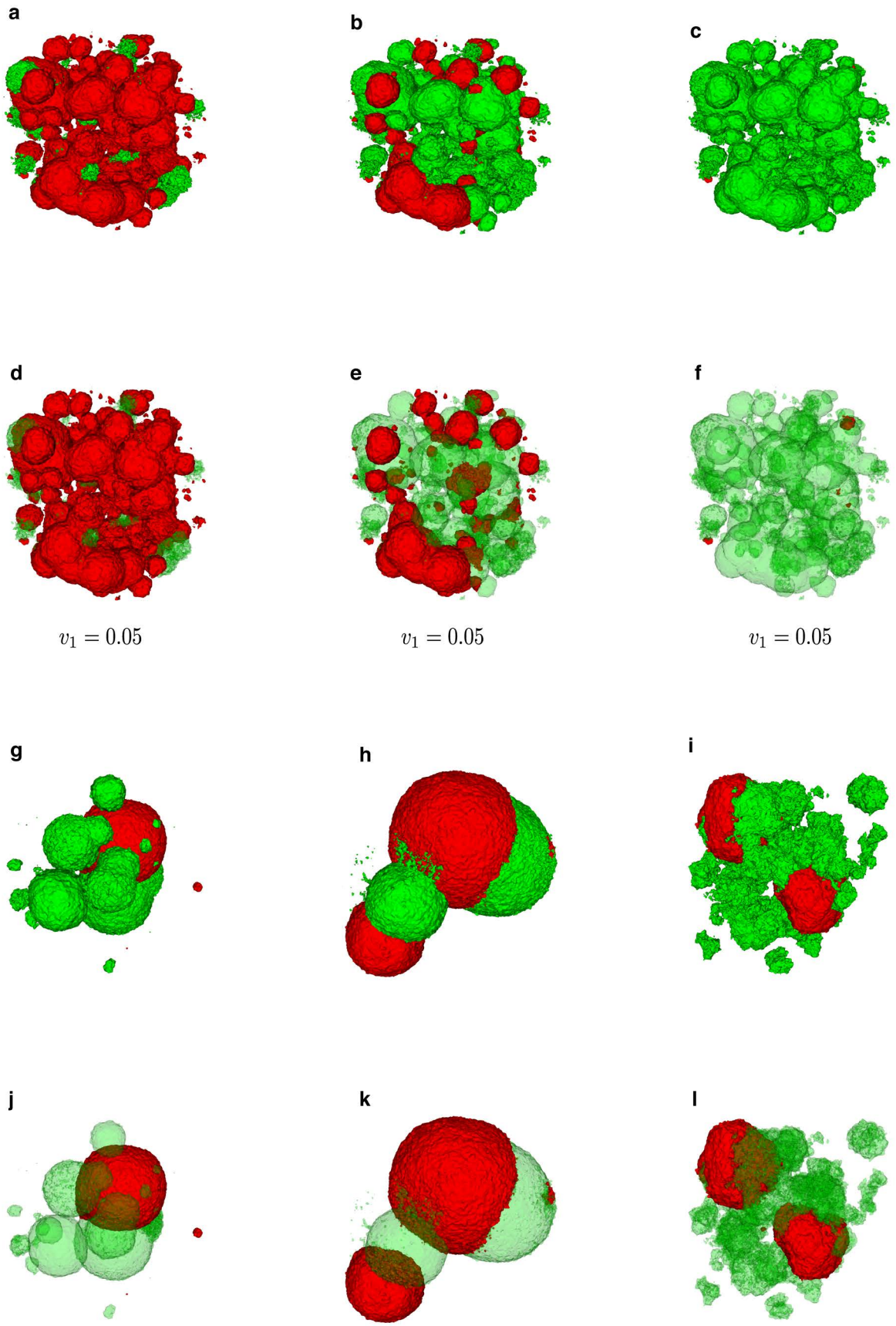
a
b
c
d
e
f
$v_1 = 0.05$
$v_1 = 0.05$
$v_1 = 0.05$
g
h
i
j
k
l
$v_1 = 5 \times 10^{-3}$
$v_1 = 5 \times 10^{-4}$
$v_1 = 5 \times 10^{-5}$

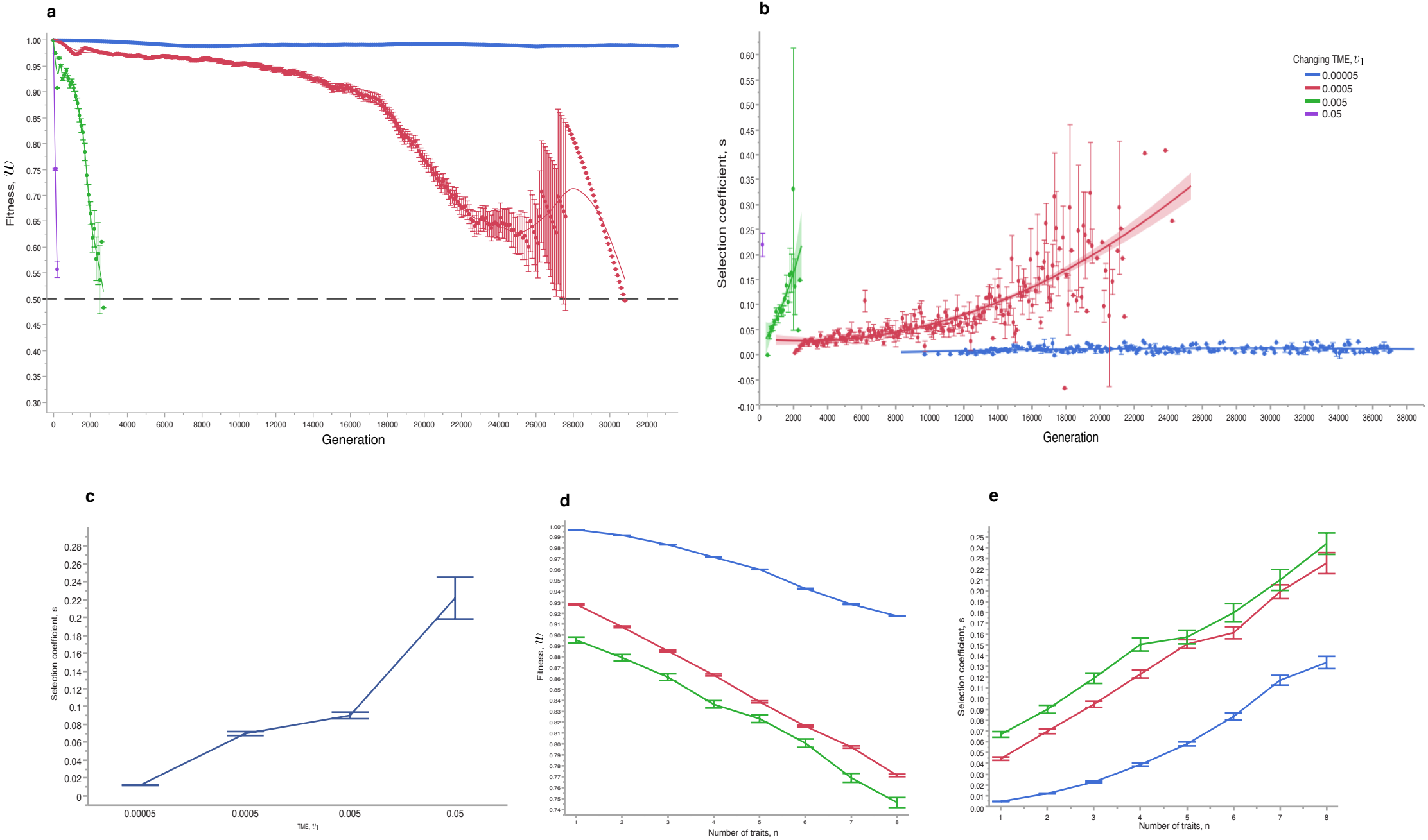
a
Fitness, $\mathcal{U}$
Generation
b
Selection coefficient, s
Generation
Changing TME, υ_1
0.00005
0.0005
0.005
0.05
c
Selection coefficient, s
TME, υ_1
0.00005
0.0005
0.005
0.05
d
Fitness, $\mathcal{U}$
Number of traits, n
e
Selection coefficient, s
Number of traits, n

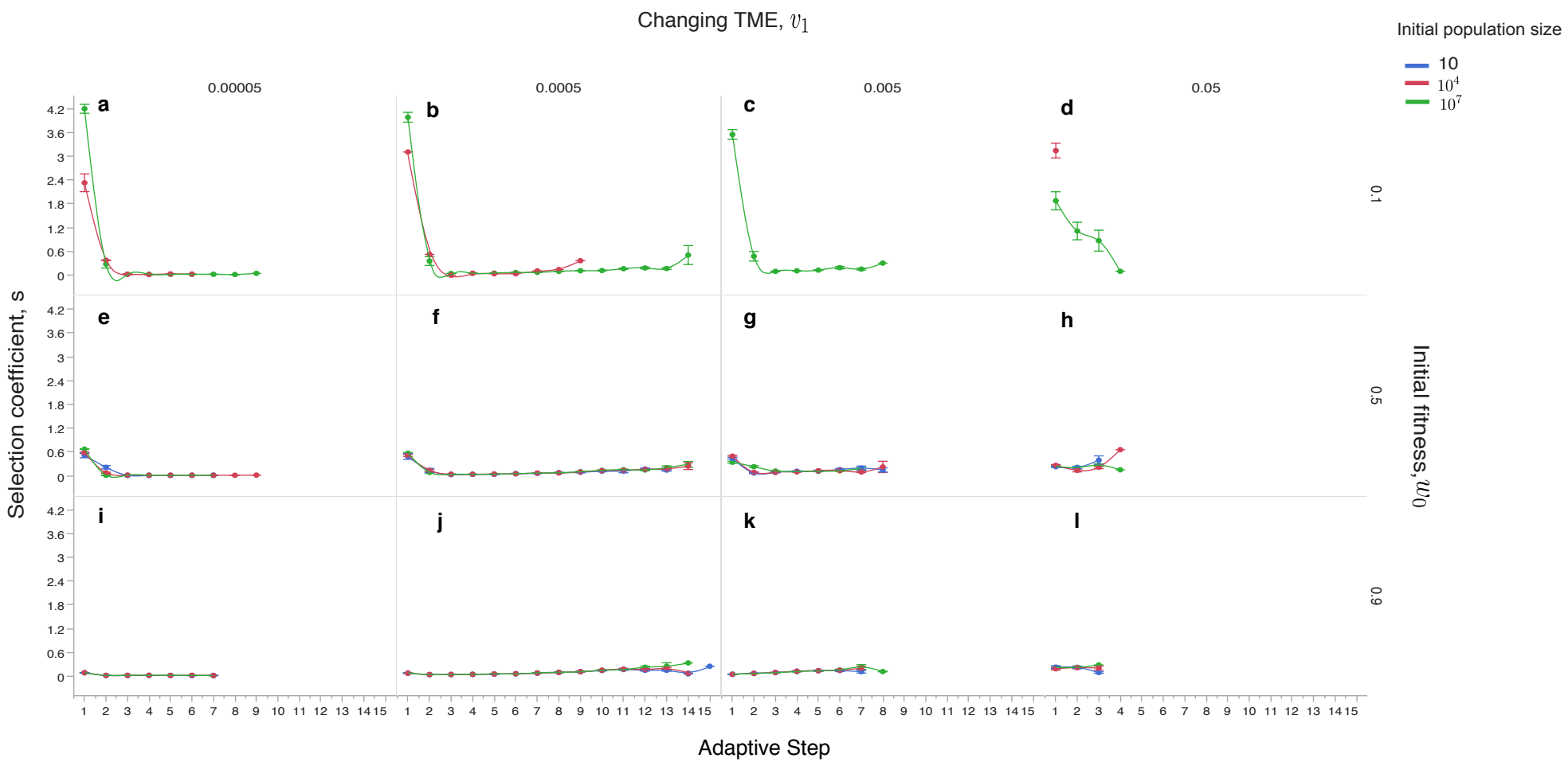
Changing TME, v_1
Initial population size
10
10^4
10^7
0.00005
0.0005
0.005
0.05
0.1
0.5
0.9
Initial fitness, u_0
Selection coefficient, s
Adaptive Step
a
b
c
d
e
f
g
h
i
j
k
l

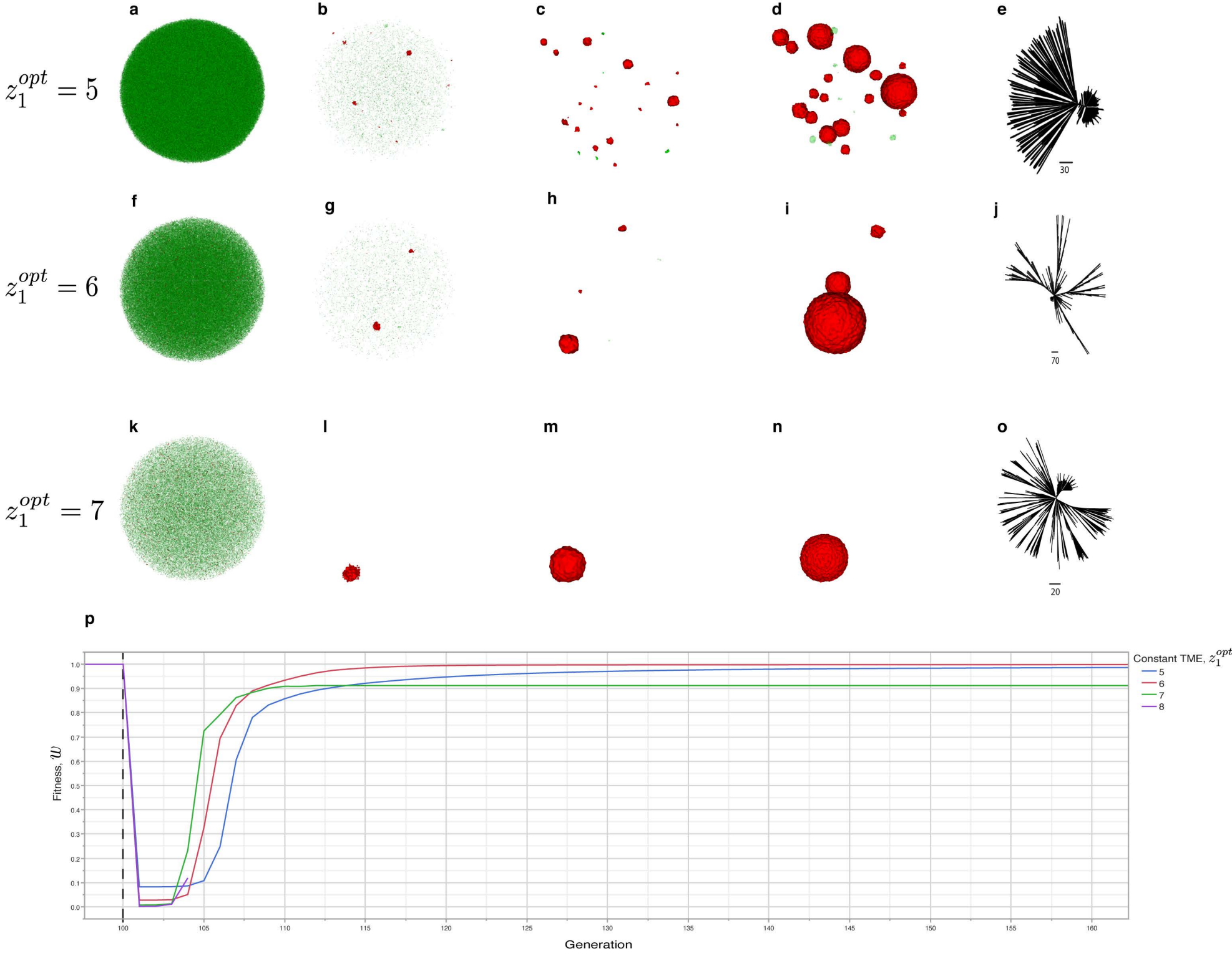
a
b
c
d
e
$z_1^{opt} = 5$
30
f
g
h
i
j
$z_1^{opt} = 6$
70
k
l
m
n
o
$z_1^{opt} = 7$
20
p
Fitness, w
Generation
Constant TME, z_1^{opt}
5
6
7
8